applied sciences

MDPI

Article

A Wearable Microphone Array Helmet for Automotive Applications

Daniel Pinardi [1], Andrea Toscani [2,*], Marco Binelli [1], Angelo Farina [1] and Jong-Suh Park [3]

[1] Department of Engineering for Industrial Systems and Technologies, University of Parma, 43124 Parma, Italy; daniel.pinardi@unipr.it (D.P.); marco.binelli@unipr.it (M.B.); angelo.farina@unipr.it (A.F.)
[2] Department of Engineering and Architecture, University of Parma, 43124 Parma, Italy
[3] Automotive R&D Division, Hyundai Motor Company, Namyang-eup, Hwaseong-si 18280, Gyeongi-do, Republic of Korea; jspark@hyundai.com
* Correspondence: andrea.toscani@unipr.it

Featured Application: Development of immersive infotainment and ANC systems in the automotive industry with Ambisonics audio.

Abstract: Growing interest in microphone array technology has been observed in the automotive industry and in this work, specifically, for Active Noise Control (ANC) systems. However, the human presence always limits the usage of microphone arrays in driving conditions at the driver's seat. This is often the most important position of the car cabin; a wearable microphone array is particularly interesting. In this paper, a wearable helmet microphone array is presented featuring 32 microphones arranged over the surface of a helmet, which also integrates a specially designed Analog-to-Digital (A/D) converter, delivering digital signals over the Automotive Audio Bus (A^2B). Digital signals are collected using a control unit located in the passenger compartment. The control unit can either deliver digital signals to a personal computer or analog signals to an external acquisition system, by means of Digital-to-Analog (D/A) converters. A prototype was built and acoustically characterized to calculate the beamforming filter matrix required to convert the recordings (pressure signals) into Ambisonics signals (a spatial audio format). The proposed solution was compared to the reference spherical microphone array of the last decade, demonstrating better performance in sound source localization at low frequencies, where ANC systems are mostly effective.

Keywords: active noise control (ANC); Ambisonics; Automotive Audio Bus (A^2B); beamforming; immersive audio; microphone array; spatial audio; wearable helmet

Academic Editor: Edoardo Piana

Received: 21 January 2025
Revised: 10 March 2025
Accepted: 13 March 2025
Published: 14 March 2025

Citation: Pinardi, D.; Toscani, A.; Binelli, M.; Farina, A.; Park, J.-S. A Wearable Microphone Array Helmet for Automotive Applications. *Appl. Sci.* **2025**, *15*, 3202. https://doi.org/10.3390/app15063202

1. Introduction

Microphone arrays are more and more employed for several purposes, such as electronic devices (e.g., dereverberation, speech enhancement and recognition), industries (e.g., machine condition monitoring), and even civil applications (e.g., structural health monitoring). Among these applications, the automotive industry particularly benefited from this technology, which is now used in a variety of problems. In [1], a uniform circular microphone array featuring seven capsules (of which one in the center) was employed to localize the speaker in autonomous shared vehicles. In [2,3], a spherical array with 32 capsules was used to auralize the car sound system of a large sedan. The same array was also employed in [4] to spatially evaluate the sound quality inside a car cabin, while in [5] the authors did a similar work with the Bruel and Kjaer WA-1565, a rigid spherical microphone array of 195 mm diameter, equipped with 36 capsules and 12 cameras. In [6], a uniform planar Micro electro-mechanical system (MEMS) array featuring 150 capsules was used to

detect pedestrians in an autonomous emergency braking system. Finally, K. Vasudev et al. attempted to enhance hands-free communication by integrating a microphone array into the seat belt [7]. The usage of microphone arrays for hands-free communication inside cars is widely studied and offers a large volume of the literature, among which three relevant references worth to be cited are [8–10].

Active Noise Control (ANC) is another field where microphone arrays find relevant practical applications in the automotive industry. In [11], linear and circular arrays with 4, 8, 16, or 32 capsules were employed to enhance noise cancelling inside a car cabin by means of the virtual sensing technique. A comprehensive review of virtual sensing algorithms for ANC can be found in [12]. In [13], a head-shaped array with 32 capsules and 8 cameras was used to spatially assess the effectiveness of an ANC system installed in a segment-D car. In [14], two linear arrays of 6 microphones were each used to enhance the performance of an ANC system by means of the noise source separation technique. From the previous examples, it is evident that geometry plays a crucial role when designing a microphone array. In fact, it determines the portion of space where the system exhibits optimal accuracy, such as a line, a plane, a half-space, or the full sphere. As a result, microphone arrays with a variety of shapes were observed. In [15], S. J. Patel et al. discussed the optimal design for linear arrays, while in [16] X. Wang et al. did the same for planar arrays and in [17] J. Trevino et al. for the cylindrical ones. Nevertheless, most of the microphone arrays are spherical, namely the spherical microphone array (SMA), constituted by a rigid shell; however, in some applications, open frame SMA are also employed. An in-depth analysis of the design of open frame SMA is discussed in [18,19], while four of the most relevant papers discussing design, analysis, and processing of rigid SMA are [20–23].

The dimension of the array is another key factor for the design, since the larger the array, the lower the minimum frequency where beamforming is effective [24]. Therefore, large arrays, either real or virtual [25], are required to localize noise sources at low frequency. This is particularly important when dealing with ANC systems for cars, which are mostly effective at very low frequencies, e.g., 50 Hz–400 Hz for road noise as referred in [26] and up to 1 kHz for tonal applications such as engine noise order cancelling, as referred in [27].

Another fundamental feature for microphone array design is the number of capsules, as the closer the microphones, the higher the maximum beamforming frequency, as demonstrated in [28] by B. Rafaely. Consequently, a trend toward the continuous appearance on the market of systems with an ever-increasing number of capsules was observed. The first microphone array was launched in 1978 by K. Farrar with the name "Soundfield" [29,30]. It featured four capsules positioned in the vertices of a tetrahedron; several other microphone arrays featuring four capsules have come to the market in the following decades, the last of them being the Saramonic Sr-VR in 2024. In 2009, Eingemike32 (also employed in this work) was launched by G. Elko [31], i.e., a SMA featuring 32 capsules; in 2017, the Octomic by Core Sound, featuring 8 capsules and the Zylia, another SMA featuring 19 MEMS capsules, were launched; and finally in 2023, the new Eingemike64, featuring 64 capsules was launched. In 2015, a prototype featuring 252 capsules was presented by Sakamoto et al. [32], while in 2021, Carsten et al. showed a portable array with 512 MEMS microphones [33].

The layout of the capsules over the surface of the array is at least as important. A heuristic approach was used for planar arrays in [34], while several mathematical approaches were developed for SMA, with the aim of optimizing the spatial sampling over the sphere, as well treated in [35]. In the case of equiangular sampling, the number N of required microphones is given by (1), while in the case of nearly uniform sampling, it is given by (2)

$$N = 4(O+1)^2 \tag{1}$$

$$N = 1/2(O+1)^2 \tag{2}$$

where O is the Ambisonics order. The Ambisonics theory, consisting of a Spherical Harmonics (SHs) expansion of the sound field at the recording point, was first presented by M. Gerzon in 1975 [36,37] and nowadays is widely employed for delivering spatial audio. More on the SH can be found in [38], while an exhaustive discussion of SH decomposition with SMA can be found in [39]. In the case of nearly uniform sampling, a mathematical approach called Spherical Design is commonly employed to optimize the distribution of the capsules over the surface of a rigid SMA. A spherical design is a finite set of N points on the d-dimensional unit sphere S_d such that the average value of any polynomial f of degree t or less equals the average value of f on the whole sphere [40–42]. Such a set is often also called the Spherical T-design. In [43,44], many spherical designs and their properties are presented. Other interesting distributions of points are based on regular polyhedrons, such as tetrahedron, dodecahedron, and icosahedron, with N = 4, 12, and 20, respectively. Eigenmike32, widely recognized as the reference system of the last decade and employed as a comparative target also in the presented work, features 32 capsules arranged in a truncated icosahedron over a rigid sphere of 84 mm diameter.

When selecting the type of capsule, the choice is between analog and digital transducers. Analog transducers can provide high-quality audio signals, but they come with some drawbacks, such as cumbersome wiring and susceptibility to noise interference, especially when long cables are used to connect the capsules to the Analog-to-Digital (A/D) converters. Affordable digital MEMS microphones are less affected by electrical interference, though this often comes at the expense of lower acoustic performance, such as reduced dynamic range and signal-to-noise ratio. A review of MEMS microphones can be found in [45].

In this work, a wearable microphone array is presented for the development and performance assessment of ANC systems installed on vehicles. The array solves a common limitation encountered in measuring automotive ANC systems with microphone arrays: the presence of the driver in the front left seat during road tests. The array was built by using a normal rigid helmet as a frame. The dimension of the helmet, which is larger than the microphone arrays currently available on the market, allows for shifting the frequency range of beamforming toward low frequencies, where ANC systems are mostly effective. With the shape of the helmet being almost spherical, the nearly uniform sampling theory was applied to optimize the distribution of the capsules over the surface of the array. A Spherical Design of degree t = 7 with N = 32 points was employed. The proposed solution features electret capsules connected to a miniaturized A/D converter incorporated in the helmet. The A/D converter also integrates an A^2B transceiver (see Section 2.3), allowing it to deliver digital signals over an Ethernet cable, thus ensuring immunity to electromagnetic disturbances, which are always present in a car cabin.

The proposed solution is flexible and can be used in many scenarios, such as internal combustion engines or electric vehicles, different road conditions (smooth, rough, very rough asphalt, with/without bumps are common tests performed by car makers), and speed. The only limitation is encountered with cabriolet and spider cars due to the aerodynamic noise and the unavailability of a windshield for the array helmet. If equipped with internal loudspeakers, the array helmet would find another interesting application in motor sport for the communication between the pilot and the co-pilot in rally competitions. Thanks to the beamforming capability, the array helmet can focus on the speaker voice, rejecting the noise and enhancing the intelligibility of the instructions provided by the co-pilot. This application is known as Audio Augmented Reality (AAR) or augmented listening. Despite no previous works being found in motor sports applications, in [46], several wearable microphone arrays, both rigid and flexible, were built and tested for AAR.

The paper is arranged as follows: Section 2 describes the development of the helmet (Section 2.1), the acoustic characterization (Section 2.2), and the architecture of the electronics (Section 2.3); Section 3 illustrates the main findings obtained within this work; in Section 4 the results are discussed; and finally, Section 5 summarizes the conclusions, the limitations, and possible future developments.

2. Materials and Methods

2.1. Array Helmet Design

The first step of the development consisted of the choice of the helmet. It must be as spherical as possible, with a smooth surface without holes, grids, vents, knobs, and protruding parts to avoid any practical limitation for capsule mounting. This led to the choice of the model X3000 by the Italian manufacturer AGV (Vicenza, Italy).

The microphonic capsule chosen to build the array is AOM-5024L-HD-R from PUI Audio (Fairborn, OH, USA), whose technical specifications are reported in Table 1. It has a very low self-noise of just 14 dB(A) and more than 90 dB(A) of dynamic range. In Figure 1 (provided by the manufacturer), one can note that the frequency response is almost flat in the interested frequency range, which is 20 Hz–1 kHz.

Table 1. Microphonic capsule specification (AOM-5024L-HD-R).

Characteristic	Value
Diameter	9.7 mm
Height	5 mm
Type	Analogue, electret
Directivity	Omnidirectional
Freq. range	20 Hz–10 kHz
Self-noise	14 dB (A)
Max SPL	110 dB

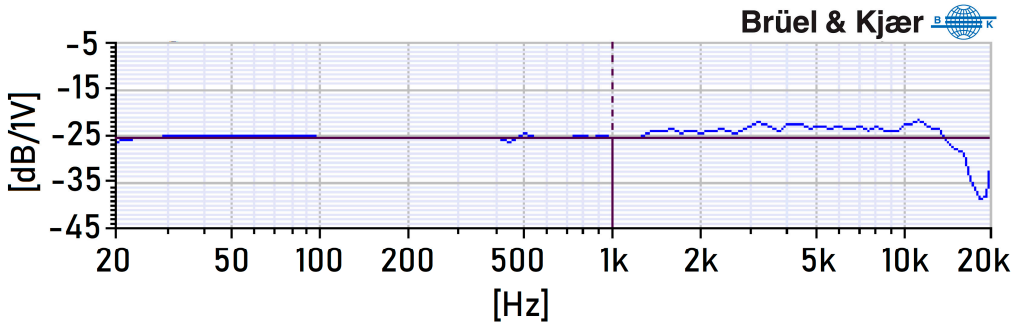

Figure 1. Frequency response of the PUI Audio AOM-5024L-HD-R capsule.

A 3D model of the helmet was acquired with the laser scanning technique by employing a Shining 3D EinScan H2. The result was stored as a stereolithography file, namely stl (also referred to as standard triangle language or standard tessellation language). In this way, it was possible to easily import and manipulate the geometry in MATLAB (R2024b). To define the optimal distribution of the capsules, the nearly uniform sampling was adopted. First, the geometrical center of the model was calculated, then 32 straight lines were propagated from the center in the same directions of a spherical design of degree $t = 7$, with N = 32 points. This configuration, as well as many others up to $t = 21$ and $N = 240$, can be found in [47]. The bundle of lines was rotated to minimize the intersections with the areas where it was not possible to mount any capsules, namely the visor and the hole for the neck. The minimum number of unallowed points was six: two on the visor and four on the neck. These points were manually repositioned. Finally, 10 mm diameters holes were

drilled by using a computer numerical control (CNC) machine and the capsules were fixed in positions by using a special adhesive modeling paste.

2.2. Acoustics Characterization of the Array Helmet

Once assembled, the helmet was characterized in the acoustics laboratory at the University of Parma, Parma (Italy), with the dimensions 5 × 3 × 8 m (W × H × L). The measurement procedure made use of a two-axis turntable and a loudspeaker (studio monitor type 8351a, by Genelec, Iisalmi, Finland) in a fixed position (Figure 2). Since the helmet must be used in a small environment, the measurement was performed at a very short distance, d = 0.5 m, to consider the near-field effect provided by the curvature of the sound waves. In fact, the commonly employed analytical beamformers rely on the plane wave hypothesis, which is only true in a far field condition, as demonstrated in [48]. This assumption is not true inside a car cockpit, due to its limited size compared to the wavelengths interested in an ANC system. The near-field beamforming [49,50] allows us to overcome the far field limitation of analytical beamformers. The test signal employed for the measurement was an Exponential Sine Sweep (ESS) [51], pre-equalized for flatting the spectrum and to reduce the time domain impulse response (IR).

Figure 2. Side view of the array helmet after assembling the capsules (**left**). A view of the array helmet mounted on the two-axis turntable while performing the acoustic characterization (**right**).

Since the loudspeaker was positioned in the center of the laboratory, the time of arrival t_1 of the first reflections (floor and ceilings) can be easily calculated as

$$t_1 = \frac{\sqrt{H^2 + d^2}}{c} \tag{3}$$

where H = 3 m is the height of the room, d = 0.5 m is the distance between the microphone array and the loudspeaker, and c = 343 m/s is the sound celerity in air at 20 °C. Note that the numerator of (3) is the total travel path of the first reflections, which is about 3.04 m, and hence $t_1 \cong 8.9$ ms or 427 samples at the standard audio sampling frequency f_s = 48 kHz. As can be seen in Figure 3, the effective number of samples between the direct sound (first peak of the IR, occurring after 70 samples) and the first reflections (second peak of the IR, occurring after 491 samples) corresponds almost exactly to the analytically calculated time of flight. Therefore, the entire direct sound can be isolated before the first reflections occur, and this technique is referred as a "pseudo-anechoic chamber" [52]. It can also be seen that the delay of the first peak in samples, s_d, perfectly matches the source–microphone distance, as follows:

$$s_d = \frac{d}{f_s} \cdot c \tag{4}$$

with $d = 0.5$ m, $f_s = 48$ kHz, and $c = 343$ m/s, it results in $s_d = 70$ samples, as expected.

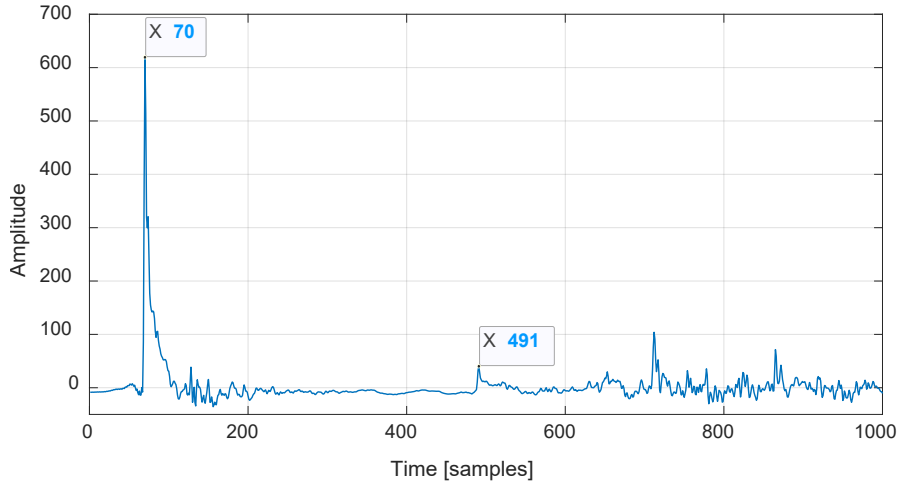

Figure 3. Pre-equalized loudspeaker IR.

In Figure 4, the spectrum of the IR direct sound is shown in the frequency range of interest, that is 20 Hz–1 kHz. Taking the lowest IR level in this range as an acceptance threshold, i.e., 85.6 dB, we can assess that the measurement can be used above 40 Hz (black dot in Figure 4). However, this can be further improved by measuring the array in a true anechoic chamber, where the IR can be kept longer thanks to the absence of reflections. In that case, without the pre-equalization filter, the lower limit would be given by the frequency response of the loudspeaker (32 Hz according to manufacturer's datasheet).

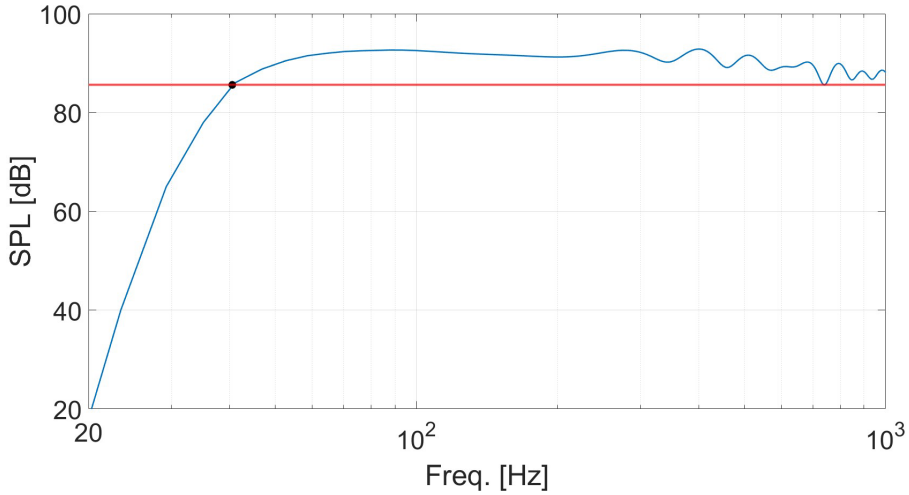

Figure 4. Spectrum of the direct sound of the pre-equalized IR.

At each repetition of the measurement, the helmet is automatically rotated by the turntable in a specific direction, and the test signal is recorded by the N capsules of the array. This procedure also addresses the problem of spatial sampling of a sphere, since the choice of the measurement directions has a strong impact on the quality of the beamforming filters. This problem was already treated by one of the same authors in [53], where it is shown that a nearly uniform sampling is again a wise choice. A set of $D = 240$ directions was used to characterize the acoustic response of the array helmet, corresponding to a spherical design of degree $t = 21$.

The measurement procedure provides the matrix $\boldsymbol{C}$ of Equation (5), which consists of the regularized Kirkeby inversion [54], a linear processing employed to compute a

beamforming matrix of Finite Impulse Response (FIR) filters. In the frequency domain, it is defined as

$$\boldsymbol{H} = [\boldsymbol{C}^* \cdot \boldsymbol{C} + \beta \cdot \boldsymbol{I}]^{-1} \cdot \left[\boldsymbol{C}^* \cdot \boldsymbol{A} \cdot e^{-j\pi k}\right] \quad (5)$$

where $\boldsymbol{C}$ is the frequency response of the array for the N capsules, D directions, and K frequencies, * is the Hermitian transpose, $\cdot$ is the scalar product, β is a parameter that varies with frequency for regularized inversion [55], $\boldsymbol{I}$ is the identity matrix, $^{-1}$ is the pseudo-inverse, $e^{-j\pi k}$ introduces a delay to guarantee the causality of the filters, and k is the frequency. Matrix $\boldsymbol{A}$ represents the desired directivity patterns of the virtual microphones encoded by the beamformer. It does not depend on the frequency and must be defined by the user for each measured direction of the matrix $\boldsymbol{C}$ and for all the N capsules. In our case, $\boldsymbol{A}$ must define the first 16 Spherical Harmonics (SHs) employed by the Ambisonics format at order 3. The 3D polar patterns of these SH are shown in Figure 5, while (6) provides the relation between Ambisonics order O and the number V of SH, as follows:

$$V = (O+1)^2 \quad (6)$$

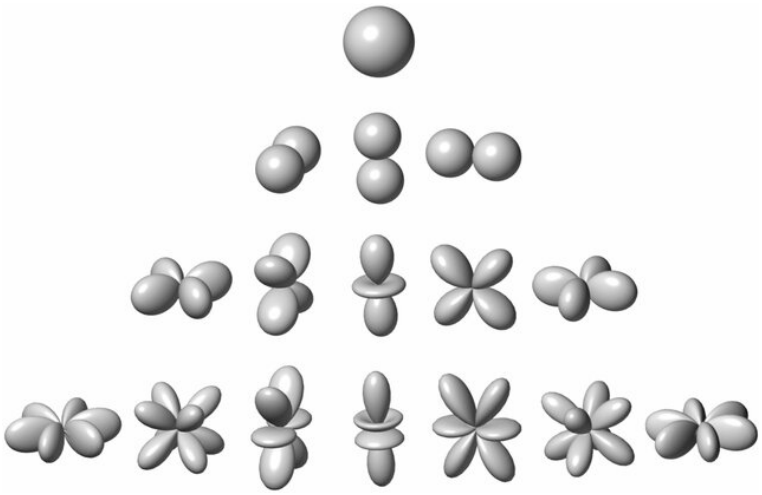

Figure 5. Ideal 3D directivity of the first v = 16 Spherical Harmonics (Ambisonics 3rd order).

The virtual microphones, i.e., SH, are then obtained by means of convolution, which is the multiplication in frequency domain, as follows:

$$\boldsymbol{A}' = \boldsymbol{C} \cdot \boldsymbol{H} \quad (7)$$

Note that only in the ideal case of perfect reconstruction of the SH will $\boldsymbol{A'} = \boldsymbol{A}$ result at all frequencies, while in the real case, $\boldsymbol{A'}$ will always approximate $\boldsymbol{A}$.

2.3. Electronics Design

The system, whose scheme is depicted in Figure 6, is composed of a helmet and a digital-to-analog (D/A) box. The helmet houses microphones and the electronic board to collect the signals, while the D/A box is connected either to a personal computer (PC) or an external acquisition system. When a PC is employed, the entire system (after A/D conversion) is full-digital, while a double A/D and D/A conversion is introduced when an external recording system is employed. However, this solution guarantees a robust signal-to-noise (S/N) ratio even inside a car cockpit, which is always electrically noisy.

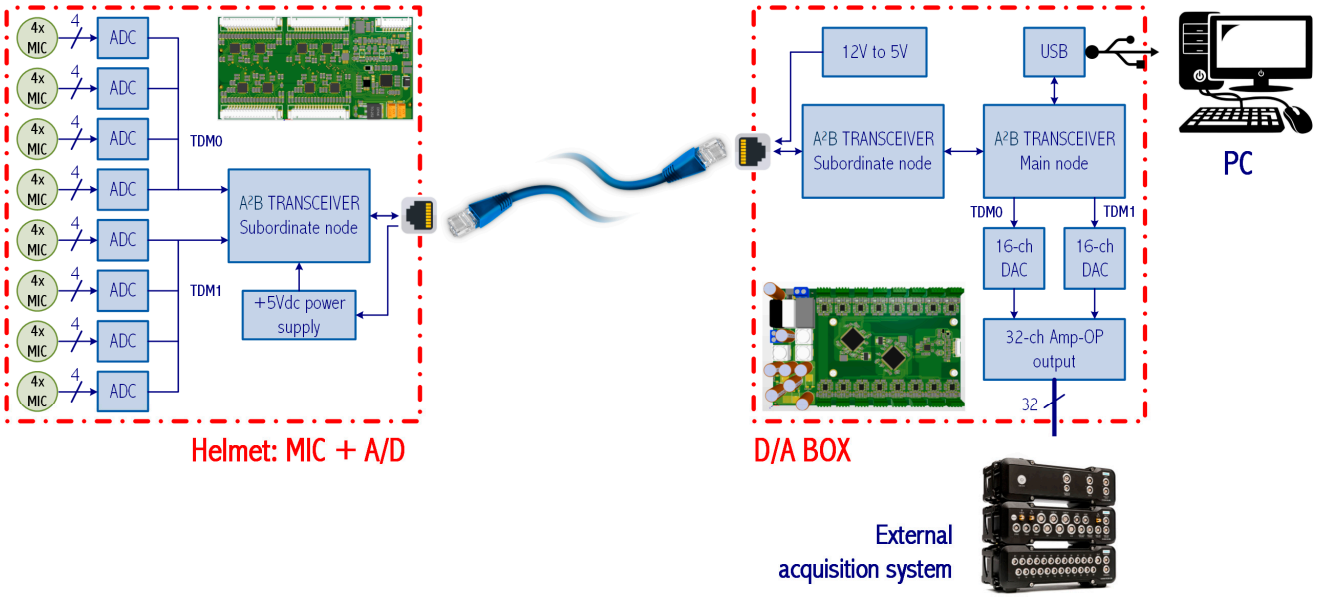

Figure 6. Block scheme of entire system: A/D board installed inside the helmet (**left**), D/A box (**right**).

The system was designed to use the A^{2}B bus by Analog Devices [56], which can handle up to 32 channels on a single Unshielded Twisted Pair (UTP), up to 15 m distance. An A^{2}B network consists of a main node and up to 10 subordinate nodes arranged in daisy-chain. Dedicated transceivers handle bus access and data flow, eliminating the need for extra devices that would increase the cost and complexity of the system. An A^{2}B network provides a bandwidth of 50 Mbit/s, enabling the transmission of up to 32 channels at the standard sample rate of 48 kHz with 16-, 24-, or 32-bits resolutions. This digital bus is particularly suitable for transmitting audio signals in both microphone arrays [57] and loudspeaker arrays [58], since it guarantees a deterministic latency of just two samples at 48 kHz and the synchronization between all the channels [59].

The electronic board installed in the helmet is provided with eight 4-channels, 16 bits, audio A/D converters, and type TLV320ADC6140 by Burr-Brown, and it also integrates the A^{2}B transceiver to acquire and deliver the data via A^{2}B bus. The A/D converters (specification are reported in Table 2) are connected to the transceiver via two Time-Division Multiplexing (TDM) 4 digital lines (TDM0 and TDM1). The signals are transferred from the helmet to the D/A box unit over an Ethernet cable that also carries the 5 Vdc power supply for the board installed inside the helmet. The ethernet cable was chosen as the physical layer of the A^{2}B bus, being cheap and common, with robust connectors that are easy to insert and remove. Note that a standard Ethernet cable includes four UTP cables, of which one is used for the A^{2}B bus and one for the power supply.

The D/A box receives the digital signals from the A^{2}B bus and transmits them to a PC via Universal Serial Bus (USB) or to an external acquisition system, after the D/A conversion. This feature is of particular interest for Noise, Vibration, and Harshness (NVH) applications since standard automotive equipment, like the SCADA by Siemens, are usually required by car makers. In addition, when such systems are employed, additional sensors like accelerometers or microphones can be recorded synchronously with the helmet array, e.g., opening to the implementation of more advanced ANC algorithms. The D/A box is made of two boards: an A^{2}B main board and an A^{2}B subordinate board. The A^{2}B main board generates the A^{2}B network and provides the clock to the A^{2}B subordinate board and the USB connection to deliver digital data to a PC. The A^{2}B subordinate board features two 16-channels, 16 bits, D/A converters, type ADAU1966 by Analog Devices (specifications are resumed in Table 2), and it is provided with 32 BNC connectors to connect to external

acquisition systems. In addition, the D/A box produces all the supply voltages for the system, starting from the 12 V on-board battery of the vehicle. To isolate the system from disturbances of the vehicle's electrical system, usually noise, all the regulators are designed to ensure full galvanic insulation.

Table 2. A/D (TLV320ADC6140) and D/A (ADAU1966) converter specification.

A/D Characteristics	Value
Number and type of input channels	4-channels, analog
Dynamic range	123 dB
Total harmonic distortion + noise (THD + N)	−98 dB
Input voltage range	2 Vrms
Sample rate	8 to 768 kHz
Power consumption	9.2 mW/ch @ 48 kHz
Audio serial data interface	TDM or I^2S
D/A Characteristics	**Value**
Number of output channels	16-channels, single ended
Resolution	24 bits
Dynamic range	110 dB (A)
Total harmonic distortion + noise (THD + N)	−97 dB
Sample rate	32 to 192 kHz

3. Results

At first, the beamforming capability of the proposed array helmet was compared to the Eigenmike32. The comparison was made by using a well-established metric for microphone array assessment [60], which consists of evaluating the deviation of the directivity $\boldsymbol{A'}$ with respect to the ideal directivity defined by $\boldsymbol{A}$. This can be performed by relying on two parameters, the Spatial Correlation (SC), which sets the limit of the beamforming at high frequency and is the defined in (8), and the Level Difference (LD), which sets the limit of the beamforming at low frequency and is defined in (9) as follows:

$$\mathrm{SC} = \frac{\sum_d (A')^T \cdot A}{\sum_d \left(\sqrt{(A')^T \cdot A'} \cdot \sqrt{A^T \cdot A} \right)} \tag{8}$$

$$\mathrm{LD} = \frac{1}{D} \sum_d \frac{A^2}{A' \cdot (A')^*} \cdot [\mathrm{dB}] \tag{9}$$

The parameters are calculated for each frequency, each direction, and each virtual microphone; then, the D directions are summed, while the virtual microphones are averaged among those belonging to the same Ambisonics order. Hence, from 1 to 4 in the first order, from 5 to 9 in the second order, and from 10 to 16 in the third order. In the ideal case of perfect reconstruction of the SH, it will be SC = 1 and LD = 0 dB. However, a certain amount of deviation is always present in the real case; hence, the upper and lower frequency limits of the beamforming are usually defined by considering two thresholds: SC > 0.9 and LD > −1 dB. The results are shown in Figure 7 for Eigenmike32 and in Figure 8 for the array helmet.

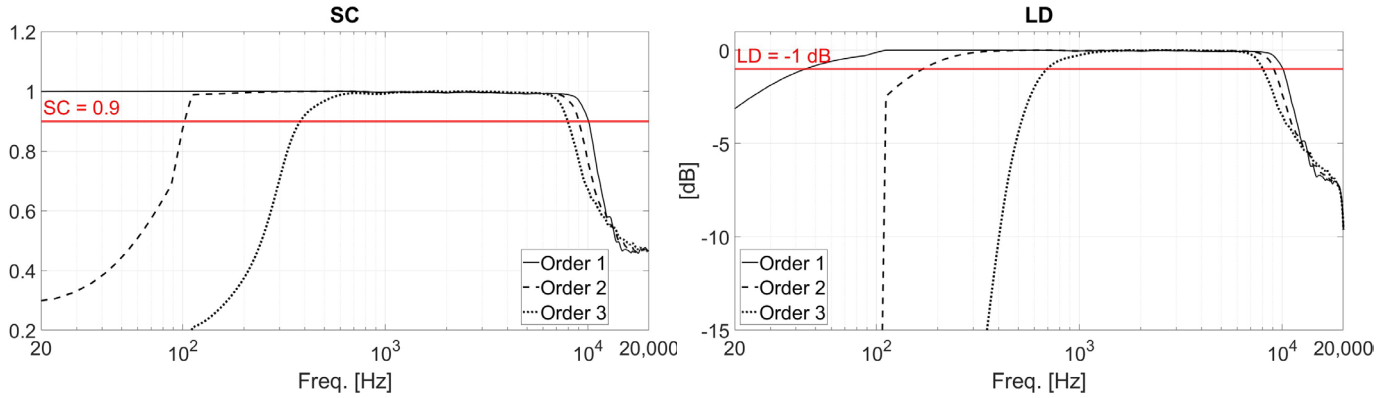

Figure 7. SC (**left**) and LD (**right**) calculated for the Eigenmike32.

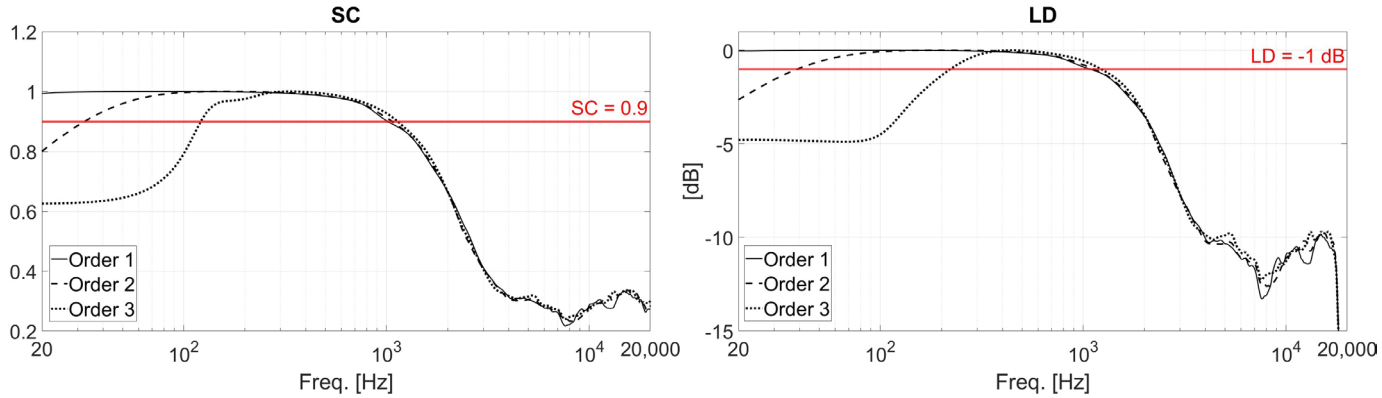

Figure 8. SC (**left**) and LD (**right**) calculated for the array helmet.

Then, a localization test was performed in the acoustic laboratory at the University of Parma, Parma (Italy), using the sound color mapping technique [61,62]. The array helmet was mounted on a microphone stand, in front of the Genelec studio monitor 8351a playing pink noise. A 30 s signal was recorded and converted into Ambisonics third order. Then, the array helmet was replaced with a dual lenses camera to take a 360° picture of the environment, which is used as the background of the sound color maps. The analysis was performed in the octave bands centered at 31.5 Hz, 63 Hz, 125 Hz, 250 Hz, 500 Hz, and 1 kHz. The quantity being mapped is the Sound Pressure Level (SPL), calculated with a resolution of 1 degree. The pseudo-color maps are generated through graphical interpolation, with a color scale that goes from blue (lowest SPL value) to red (highest SPL value). The results are shown in Figure 9.

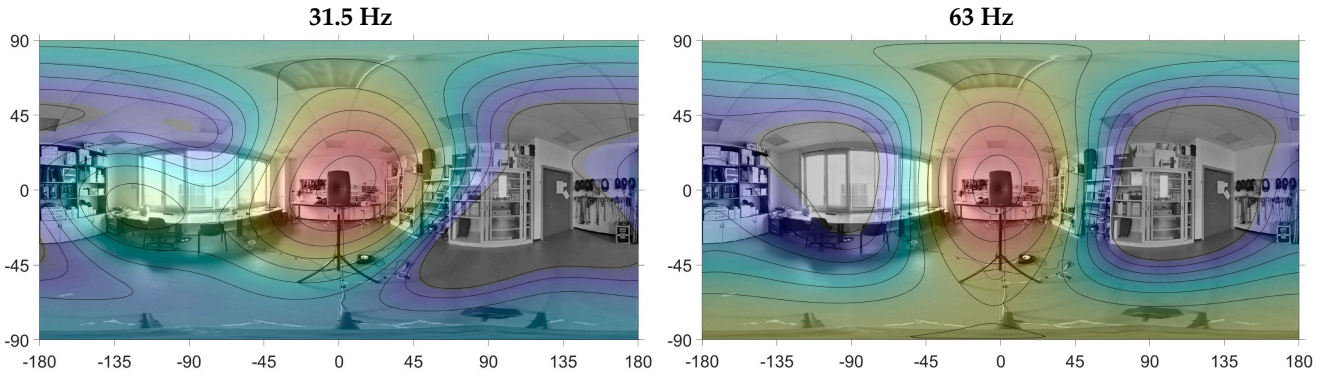

Figure 9. *Cont.*

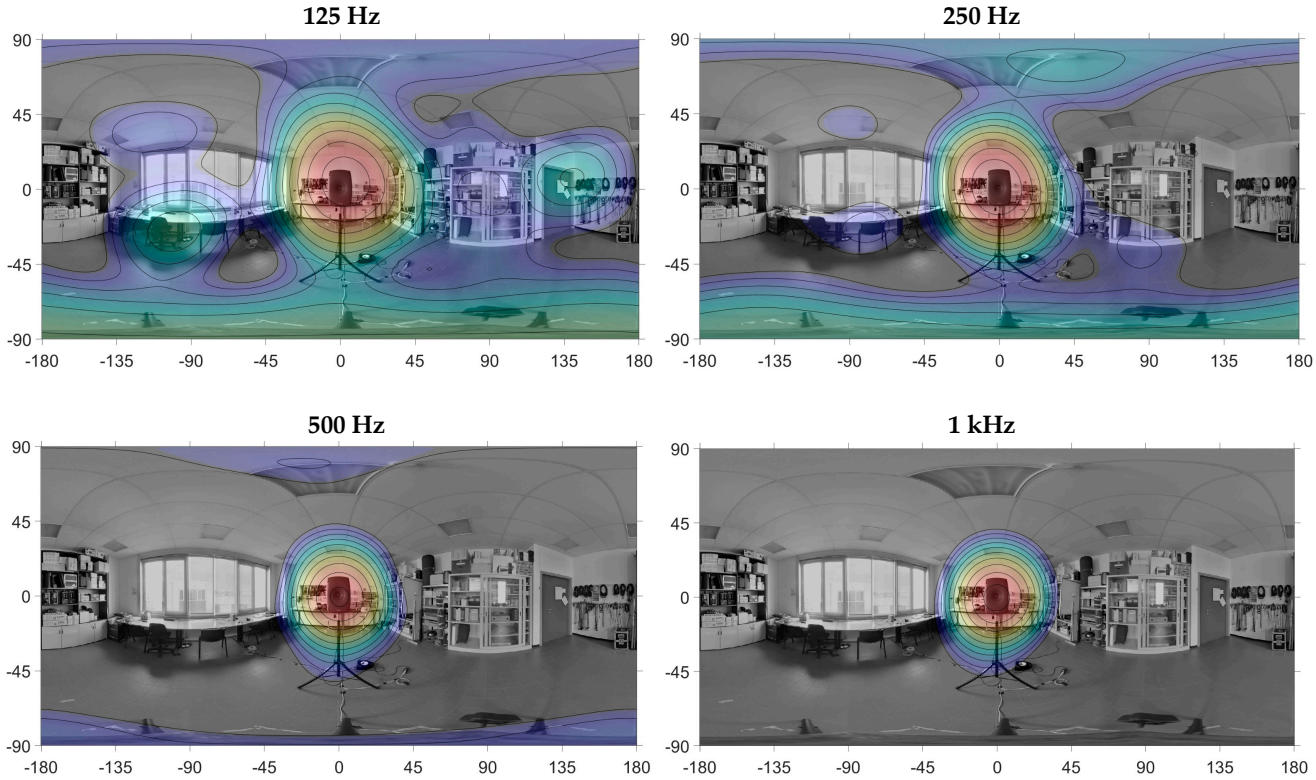

Figure 9. Sound color map analysis of a pink noise source located in (0°; 0°) at various octave bands.

4. Discussion

The SC and LD charts of Figures 7 and 8 can be used to precisely define the frequency limits of beamforming at each Ambisonics order. This is obtained by applying the previously stated thresholds, SC > 0.9 and LD > −1 dB. Each of them intersects the chart for each Ambisonics order in two points, thus identifying a low and a high acceptable frequency. These results are shown in Table 3, where it can be seen that the LD is always more restrictive at low frequency, while the SC is at high frequency. Therefore, the frequency limits provided by the two metrics must be combined, taking the most restrictive condition at low and at high frequency for each Ambisonics order (Table 4).

Table 3. Acceptable low and high frequency limits at various Ambisonics orders for SC and LD metrics.

	Eigenmike32				**Array Helmet**			
	SC		**LD**		**SC**		**LD**	
Ambisonics Order	**Low Freq. [Hz]**	**High Freq. [Hz]**	**Low Freq. [Hz]**	**High Freq. [Hz]**	**Low Freq. [Hz]**	**High Freq. [Hz]**	**Low Freq. [Hz]**	**High Freq. [Hz]**
1	-	10,000	45	10,100	-	1050	-	1100
2	100	9000	170	9100	35	1050	40	1100
3	380	7950	700	8050	120	1050	220	1100

The maximum beamforming frequency for the array helmet is 1 kHz at all orders. Despite being lower than the Eigenmike32 (10 kHz at 1st order, 9 kHz at 2nd and 8 kHz at 3rd), it is still acceptable for ANC applications. As referred to in [28] by R. Boaz, the maximum theoretical beamforming frequency, f_{max}, can be calculated as

$$f_{max} = \frac{1}{2} \cdot \frac{c}{d_{min}} \tag{10}$$

where c = 343 m/s is the celerity of the sound wave and d_{min} is the minimum distance between the capsules of the array. The results shown in Table 5 are obtained by replacing the value of d_{min} in (10) for the Eigenmike32 and for the array helmet.

Table 4. Combined frequency limits at various Ambisonics orders.

	Eigenmike32		Array Helmet	
Ambisonics Order	**Min. Freq. [Hz]**	**Max. Freq. [Hz]**	**Min. Freq. [Hz]**	**Max. Freq. [Hz]**
1	45	10,000	20 *	1050
2	170	9000	40	1050
3	700	7950	220	1050

* Theoretical value. The current practical limit is 40 Hz due to the pseudo-anechoic measurement; further improvement can be made with a true anechoic measurement.

Table 5. Theoretical maximum beamforming frequencies for Eigenmkie32 and the array helmet.

	d_{min} [mm]	Theoretical f_{max} [kHz]
Eigenmike32	17	10
Array helmet	170	1

The main advantage offered by the proposed solution consists of a significant shift in the beamforming capability toward low frequencies, as follows:

- First order Ambisonics at 20 Hz (array helmet) instead of 45 Hz (Eingemike32);
- Second order Ambisonics at 40 Hz (array helmet) instead of 170 Hz (Eingemike32);
- Third order Ambisonics at 220 Hz (array helmet) instead of 700 Hz (Eingemike32).

Usually, the comparison between microphone arrays is also performed in terms of octave bands. As can be seen in Table 6, the array helmet allowed gaining one Ambisonics order at the octave bands from one to five. The two solutions have the same performance at the sixth octave band (centered at 1 kHz), while only the Eigenmike32 operates at the octave bands centered at 2, 4, and 8 kHz. A particularly useful improvement for ANC applications is obtained at the first octave band (centered at 31.5 Hz), at which the Eigenmike32 does not provide any beamforming, while the array helmet offers a first order localization.

Table 6. Ambisonics orders at different octave bands.

Octave Bands Center Frequency [Hz]	**Highest Available Ambisonics Order**	
	Eigenmike32	**Array Helmet**
31.5	-	1
63	1	2
125	1	2
250	2	3
500	2	3
1000	3	3
2000	3	-
4000	3	-
8000	3	-
16,000	-	-

The second laboratory experiment, related to the localization of a noise source through sound color mapping, is now analyzed. The acoustic center of noise source was positioned coincident with the optical center of the panoramic camera. Therefore, in polar coordinates

(azimuth, a, and elevation, e) the acoustic center is in $a = 0°$; $e = 0°$. Table 7 shows the estimated position of the direction of arrival (DoA) of the direct sound, in polar coordinates. The DoA of the direct sound was estimated in correspondence of the maximum SPL, which is the center of the red spots in the color maps of Figure 9.

Table 7. Polar coordinates of the DoA of the direct sound at different octave bands for the array helmet.

Octave Bands Center Frequency [Hz]	Estimated DoA of Direct Sound Located at (0°; 0°)	
	Azimuth [°]	Elevation [°]
31.5	0	1
63	−2	3
125	3	4
250	−1	1
500	1	−1
1000	0	−1

As can be seen, an average absolute error of 1.2° is made along the azimuth and 1.8° along the elevation. The array helmet correctly localized the sound source (Genelec studio monitor) even at the first octave band, where only the first order Ambisonics is available. At 125 Hz, when the second order Ambisonics becomes available, some reflections can also be seen, e.g., the door (135°; 0°) and the desk (−100°; −30°). Above 250 Hz, the third order Ambisonics provides its own contribution too, and the spot on the noise source becomes narrower as the frequency increases.

5. Conclusions

A wearable helmet microphone array featuring 32 electret capsules has been developed, built, and characterized. It integrates a miniaturized 32-channel A/D converter, which avoids the bulky wiring that would occur with an analog solution and ensures a high S/N ratio thanks to the usage of the A^2B digital bus. In addition, this solution allows only one Ethernet cable to come out of the helmet, maintaining good comfort and ease of use. The A^2B signal is received by an external D/A box, which can deliver digital data to the PC via USB or convert the data back to the analog domain by means of two D/A converters, allowing us to record them with an external acquisition unit.

The array helmet was compared with the Eigenmike32, a spherical microphone array that widely considered the reference equipment for spatial audio recording during the last decade. By analyzing two metrics for Ambisonics performance evaluation, namely Spatial Correlation and Level Difference, it was possible to assess that the proposed system shifted toward low frequencies, with the Ambisonics orders by one or even two octaves, making it accurate even at the lowest octave band, centered at 31.5 Hz, where the Eigenmike32 is not effective at all. These results have been proved with a laboratory test consisting of a noise source localization problem, making use of the sound color mapping technique. The array helmet was demonstrated to correctly localize the noise source at all frequencies, with a trend of increasing accuracy with frequency, as expected. The highest valid frequency for beamforming has been reduced to 1 kHz, due to the large size of the helmet compared to the number of capsules. However, such a frequency is still above the maximum frequency at which Active Noise Control systems for cars are effective. In conclusion, the proposed solution can be employed for the assessment and the development of road noise cancelling or engine order cancelling systems at the driver seat in driving condition.

The presented array has two limitations. Most of the rolling noise from the wheels comes from below; therefore, the highest microphone density would be desired in the

lower part of the helmet to increase the spatial resolution in the interested portion of space. However, this is not possible due to the presence of the neck. The second limitation consists in the movement of the driver's head, which is naturally unstable when driving a car, in particular while cornering. Therefore, when the recording is played back, a mismatch between the orientation of the listener's head and the orientation of the sound field may occur. However, this problem will be overcome in a future update of the helmet by installing a head-tracking system to record the quaternion of spatial rotation synchronously with the pressure signals. Such a solution will allow compensating the head's movements in post-processing, by counter-rotating the sound field after Ambisonics conversion.

6. Patents

A patent request was submitted for the presented work, application number US 18/519,990.

Author Contributions: Conceptualization, A.F. and J.-S.P.; methodology, A.F.; software, D.P.; validation, D.P. and A.T.; formal analysis, A.F.; investigation, A.T. and D.P.; resources, J.-S.P.; data curation, D.P.; writing—original draft preparation, D.P. and A.T.; writing—review and editing, A.F., A.T., M.B. and J.-S.P.; visualization, D.P.; supervision, A.F.; project administration, A.F. and J.-S.P.; funding acquisition, A.F. All authors have read and agreed to the published version of the manuscript.

Funding: This research received no external funding.

Institutional Review Board Statement: Not applicable.

Informed Consent Statement: Not applicable.

Data Availability Statement: The datasets presented in this article are not readily available because they are subjected to industrial secrecy. Requests to access the datasets should be directed to jspark@hyundai.com.

Acknowledgments: The authors are grateful to Hyundai Motor Company for the economic support that made this research possible.

Conflicts of Interest: Author Jong-Suh Park was employed by the company Hyundai Motor Company. The remaining authors declare that the research was conducted in the absence of any commercial or financial relationships that could be construed as a potential conflict of interest.

Abbreviations

The following abbreviations are used in this manuscript:

A^2B	Automotive Audio Bus
A/D	Analog-to-Digital
AAR	Audio Augmented Reality
ANC	Active Noise Control
CNC	Computer Numerical Control
D/A	Digital-to-Analog
DC	Direct Current
DoA	Direction of Arrival
DSP	Digital Signal Processing
ESS	Exponential Sine Sweep
IR	Impulse Response
FIR	Finite Impulse Response
LD	Level Difference
MEMS	Micro Electro-mechanical Systems
NVH	Noise, Vibration and Harshness
PC	Personal Computer

PWD	Plane Wave Decomposition
S/N	Signal-to-Noise
SC	Spatial Correlation
SH	Spherical Harmonics
SMA	Spherical Microphone Array
SPL	Sound Pressure Level
TDM	Time-division multiplexing
USB	Universal Serial Bus
UTP	Unshielded Twisted Pair

References

1. Marques, I.; Sousa, J.; Sá, B.; Costa, D.; Sousa, P.; Pereira, S.; Santos, A.; Lima, C.; Hammerschmidt, N.; Pinto, S.; et al. Microphone Array for Speaker Localization and Identification in Shared Autonomous Vehicles. *Electronics* **2022**, *11*, 766. [CrossRef]
2. Pinardi, D.; Farina, A.; Park, J.-S. Low Frequency Simulations for Ambisonics Auralization of a Car Sound System. In Proceedings of the 2021 Immersive and 3D Audio: From Architecture to Automotive, I3DA 2021, Bologna, Italy, , 8–10 September 2021. [CrossRef]
3. Pinardi, D.; Riabova, K.; Binelli, M.; Farina, A.; Park, J.-S. Geometrical Acoustics Simulations for Ambisonics Auralization of a Car Sound System at High Frequency. In Proceedings of the 2021 Immersive and 3D Audio: From Architecture to Automotive, I3DA 2021, Bologna, Italy, 8–10 September 2021. [CrossRef]
4. Pinardi, D.; Ebri, L.; Belicchi, C.; Farina, A.; Binelli, M. *Direction Specific Analysis of Psychoacoustics Parameters Inside Car Cockpit: A Novel Tool for NVH and Sound Quality*; SAE Technical Paper 2020-01-1547; SAE International: Warrendale, PA, USA, 2020; Available online: https://saemobilus.sae.org/papers/direction-specific-analysis-psychoacoustics-parameters-inside-car-cockpit-a-novel-tool-nvh-sound-quality-2020-01-1547#citation (accessed on 12 March 2025). [CrossRef]
5. Jin, J.; Cheng, H.; Xie, T.; Lu, H. Interior Sound Field Subjective Evaluation Based on the 3D Distribution of Sound Quality Objective Parameters and Sound Source Localization. *Materials* **2021**, *14*, 429. [CrossRef] [PubMed]
6. Izquierdo, A.; del Val, L.; Villacorta, J.J. Feasibility of Using a MEMS Microphone Array for Pedestrian Detection in an Autonomous Emergency Braking System. *Sensors* **2021**, *21*, 4162. [CrossRef]
7. Rajan, V.K.; Krini, M.; Rodemer, K.; Schmidt, G. Signal processing techniques for seat belt microphone arrays. *EURASIP J. Adv. Signal Process.* **2016**, *2016*, 35. [CrossRef]
8. Nordholm, S.E.; Low, S.Y.; Dam, H.Q. A Microphone Array Solution for Duplex Hands-Free Communication Systems. In Proceedings of the 2007 Digest of Technical Papers International Conference on Consumer Electronics, Las Vegas, NV, USA, 10–14 January 2007; IEEE: New York, NY, USA, 2007; pp. 1–2. [CrossRef]
9. Oh, S.; Viswanathan, V. Microphone Array for Hands-Free Voice Communication in a Car. In *Modern Methods of Speech Processing*; Springer: Boston, MA, USA, 1995; pp. 351–375. [CrossRef]
10. Grenier, Y. A microphone array for car environments. In Proceedings of the ICASSP-92: 1992 IEEE International Conference on Acoustics, Speech, and Signal Processing, San Francisco, CA, USA, 23–26 March 1992; IEEE: New York, NY, USA, 1992; Volume 1, pp. 305–308. [CrossRef]
11. Ahamed, P.S.S.; Duraiswamy, P. Virtual Sensing Active Noise Control System with 2D Microphone Array for Automotive Applications. In Proceedings of the 2019 6th International Conference on Signal Processing and Integrated Networks (SPIN), Noida, India, 7–8 March 2019; IEEE: New York, NY, USA, 2019; pp. 151–155. [CrossRef]
12. Moreau, D.; Cazzolato, B.; Zander, A.; Petersen, C. A Review of Virtual Sensing Algorithms for Active Noise Control. *Algorithms* **2008**, *1*, 69–99. [CrossRef]
13. Pinardi, D. A Human Head Shaped Array of Microphones and Cameras for Automotive Applications. In Proceedings of the 2021 Immersive and 3D Audio: From Architecture to Automotive, I3DA 2021, Bologna, Italy, 8–10 September 2021. [CrossRef]
14. Iwai, K.; Kinoshita, S.; Kajikawa, Y. Multichannel feedforward active noise control system combined with noise source separation by microphone arrays. *J. Sound Vib.* **2019**, *453*, 151–173. [CrossRef]
15. Patel, S.J.; Grant, S.L.; Zawodniok, M.; Benesty, J. On the Design of Optimal Linear Microphone Array Geometries. In Proceedings of the 2018 16th International Workshop on Acoustic Signal Enhancement (IWAENC), Tokyo, Japan, 17–20 September 2018; IEEE: New York, NY, USA, 2018; pp. 501–505. [CrossRef]
16. Wang, X.; Li, M.; Zhao, Y.; Wang, J.; Tan, X. Design of Planar Differential Microphone Array Beampatterns with Controllable Mainlobe Beamwidth and Sidelobe Level. *Sensors* **2023**, *23*, 3733. [CrossRef]
17. Trevino, J.; Koyama, S.; Sakamoto, S.; Suzuki, Y. Mixed-order Ambisonics encoding of cylindrical microphone array signals. *Acoust. Sci. Technol.* **2014**, *35*, 174–177. [CrossRef]

18. Du, C.; Leclere, Q.; Li, B. Design And Evaluation of Open Spherical Microphone Arrays. In Proceedings of the 24th International Congress on Sound And Vibration (ICSV24), London, UK, 23–27 July 2017; HAL Open Science: London, UK, 2017.
19. Yang, B.; Shi, S.; Yang, D. Acoustic source localization using the open spherical microphone array in the low-frequency range. *MATEC Web Conf.* **2019**, *283*, 04001. [CrossRef]
20. González, R.; Pearce, J.; Lokki, T. Modular design for spherical microphone arrays. In Proceedings of the AES International Conference, Tokyo, Japan, 7–9 August 2018; p. 1. Available online: http://www.aes.org/e-lib/browse.cfm?elib=19701 (accessed on 12 March 2025).
21. Fernandez-Grande, E. Sound field reconstruction using a spherical microphone array. *J. Acoust. Soc. Am.* **2016**, *139*, 1168–1178. [CrossRef]
22. Rafaely, B. Analysis and design of spherical microphone arrays. *IEEE Trans. Speech Audio Process.* **2005**, *13*, 135–143. [CrossRef]
23. Gover, B.N.; Ryan, J.G.; Stinson, M.R. Designing a Spherical Microphone Array for the Directional Analysis of Reflections and Reverberation. In Proceedings of the Audio Engineering Society Convention 115, New York, NY, USA, 10–13 October 2003; Available online: http://www.aes.org/e-lib/browse.cfm?elib=12447 (accessed on 12 March 2025).
24. Sachar, J.M.; Silverman, H.F.; Patterson, W.R. Large vs small aperture microphone arrays: Performance over a large focal area. In Proceedings of the 2001 IEEE International Conference on Acoustics, Speech, and Signal Processing. Proceedings (Cat. No.01CH37221), Salt Lake City, UT, USA, 7–11 May 2001; IEEE: New York, NY, USA, 2001; pp. 3049–3052. [CrossRef]
25. Yang, B.; Gao, Y.; Guo, Q.; Shi, S. A Low Frequency Noise Source Localization and Identification Method Based on a Virtual Open Spherical Vector Microphone Array. *Appl. Sci.* **2023**, *13*, 4368. [CrossRef]
26. Tripodi, C.; Costalunga, A.; Ebri, L.; Vizzaccaro, M.; Cattani, L.; Ugolotti, E.; Nili, T. Experimental Results on Active Road Noise Cancellation in Car Interior. In Proceedings of the Audio Engineering Society Convention 144, Milan, Italy, 23–26 May 2018; Available online: http://www.aes.org/e-lib/browse.cfm?elib=19493 (accessed on 12 March 2025).
27. Ferrari, C.L.; Cheer, J.; Mautone, M. Investigation of an engine order noise cancellation system in a super sports car. *Acta Acust.* **2023**, *7*, 1. [CrossRef]
28. Rafaely, B. Fundamentals of Spherical Array Processing. In *Springer Topics in Signal Processing*; Springer International Publishing: Cham, Switzerland, 2019. [CrossRef]
29. Farrar, K. Soundfield microphone 2—Detailed functioning of control unit. *Wirel. World* **1979**, *85*, 99–103.
30. Farrar, K. Soundfield microphone—Design and development of microphone and control unit. *Wirel. World* **1979**, *85*, 48–50.
31. Meyer, J.; Elko, G. A highly scalable spherical microphone array based on an orthonormal decomposition of the soundfield. In Proceedings of the IEEE International Conference on Acoustics Speech and Signal Processing, Orlando, FL, USA, 13–17 May 2002; IEEE: New York, NY, USA, 2002; pp. II-1781–II-1784. [CrossRef]
32. Sakamoto, S.; Hongo, S.; Okamoto, T.; Iwaya, Y.; Suzuki, Y. Sound-space recording and binaural presentation system based on a 252-channel microphone array. *Acoust. Sci. Technol.* **2015**, *36*, 516–526. [CrossRef]
33. Spehr, C.; Ernst, D.; Raumer, H.-G. MEMS microphone intensity array for cabin noise measurements. In Proceedings of the INTER-NOISE and NOISE-CON Congress and Conference Proceedings, Washington, DC, USA, 1–5 August 2021; Volume 263, pp. 3023–3034. [CrossRef]
34. Kodrasi, I.; Rohdenburg, T.; Doclo, S. Microphone position optimization for planar superdirective beamforming. In Proceedings of the 2011 IEEE International Conference on Acoustics, Speech and Signal Processing (ICASSP), Prague, Czech Republic, 22–27 May 2011; IEEE: New York, NY, USA, 2011; pp. 109–112. [CrossRef]
35. Ciric, D.; Djordjevic, A.; Licanin, M. Analysis of effects of spherical microphone array physical parameters using simulations. *Facta Univ.-Ser. Electron. Energet.* **2013**, *26*, 107–119. [CrossRef]
36. Gerzon, M. Ambisonics. Part two: Studio techniques. *Studio Sound* **1975**, *17*, 24–30. Available online: https://www.michaelgerzonphotos.org.uk/articles/Ambisonics%202.pdf (accessed on 12 March 2025).
37. Gerzon, M.A. The Design of Precisely Coincident Microphone Arrays for Stereo and Surround Sound. In Proceedings of the Audio Engineering Society Convention 50, London, UK, 4–7 March 1975; Available online: http://www.aes.org/e-lib/browse.cfm?elib=2466 (accessed on 12 March 2025).
38. Ferres, N.M. *An Elementary Treatise on Spherical Harmonics and Subjects Connected with Them*; Cornell University Library: Ithaca, NY, USA, 1877.
39. Battista, G.; Chiariotti, P.; Castellini, P. Spherical Harmonics Decomposition in inverse acoustic methods involving spherical arrays. *J. Sound Vib.* **2018**, *433*, 425–460. [CrossRef]
40. Colbourn, C.J.; Dinitz, J.H. (Eds.) *Handbook of Combinatorial Designs*; Chapman and Hall/CRC: Boca Raton, FL, USA, 2006. [CrossRef]
41. Bannai, E. Rigid spherical t-designs and a theorem of Y. Hong. *J. Fac. Sci. Univ. Tokyo* **1987**, *34*, 485–489.
42. Bannai, E.; Bannai, E. A survey on spherical designs and algebraic combinatorics on spheres. *Eur. J. Comb.* **2009**, *30*, 1392–1425. [CrossRef]
43. Bannai, E.; Damerell, R.M. Tight spherical designs, I.J. *Math. Soc. Jpn.* **1979**, *31*, 199–207. [CrossRef]

44. Bannai, E.; Okuda, T.; Tagami, M. Spherical designs of harmonic index *t*. *J. Approx. Theory* **2015**, *195*, 1–18. [CrossRef]
45. Zawawi, S.A.; Hamzah, A.A.; Majlis, B.Y.; Mohd-Yasin, F. A Review of MEMS Capacitive Microphones. *Micromachines* **2020**, *11*, 484. [CrossRef]
46. Corey, R.M. Microphone Array Processing for Augmented Listening. Ph.D. Thesis, University of Illinois, Urbana, IL, USA, 2019.
47. Hardin, R.H.; Sloane, N.J.A. McLaren's improved snub cube and other new spherical designs in three dimensions. *Discret. Comput. Geom.* **1996**, *15*, 429–441. [CrossRef]
48. Shen, J.; Jia, X. Diffraction of a plane wave by an infinitely long circular cylinder or a sphere: Solution from Mie theory. *Appl. Opt.* **2013**, *52*, 5707–5712. [CrossRef]
49. Ryan, J.G.; Goubran, R.A. Near-field beamforming for microphone arrays. In Proceedings of the 1997 IEEE International Conference on Acoustics, Speech, and Signal Processing, Munich, Germany, 21–24 April 1997; IEEE Computer Society Press: Los Alamitos, CA, USA, 1997; pp. 363–366. [CrossRef]
50. Pinardi, D. Spherical Wave Diffraction for Microphone Arrays Operating in Near Field. In Proceedings of the 2023 Immersive and 3D Audio: From Architecture to Automotive, I3DA 2023, Bologna, Italy, 5–7 September 2023.
51. Otero, J.; Felis, I. Measurement Transducer Impulse Response Using an Exponential Sine Sweep Method. *Proceedings* **2019**, *4*, 53. [CrossRef]
52. Denk, F.; Kollmeier, B.; Ewert, S.D. Removing Reflections in Semianechoic Impulse Responses by Frequency-Dependent Truncation. *J. Audio Eng. Soc.* **2018**, *66*, 146–153. [CrossRef]
53. Pinardi, D.; Farina, A.; Binelli, M. Transducer Distribution on Spherical Arrays for Ambisonics Recording and Playback. In Proceedings of the 2023 Immersive and 3D Audio: From Architecture to Automotive (I3DA), Bologna, Italy, 5–7 September 2023; IEEE: New York, NY, USA, 2023; pp. 1–9. [CrossRef]
54. Kirkeby, O.; Orduna, F.; Nelson, P.A.; Hameda, H. Inverse Filtering in Sound Reproduction. *Meas. Control* **1993**, *26*, 261–266. [CrossRef]
55. Tokuno, H.; Kirkeby, O.; Nelson, P.A.; Hamada, H. Inverse Filter of Sound Reproduction Systems Using Regularization. *IEICE Trans Fundam. Electron. Commun. Comput. Sci.* **1997**, *E80-A*, 809–820. Available online: https://www.melaudia.net/zdoc/kirkebyInverseFilter.PDF (accessed on 12 March 2025).
56. Devices, A. A2B Audio Bus: An Easier, Simpler Solution for Audio Design. Available online: https://www.analog.com/en/applications/technology/a2b-audio-bus.html (accessed on 12 March 2025).
57. Pinardi, D.; Toscani, A.; Binelli, M.; Saccenti, L.; Farina, A.; Cattani, L. Full-Digital Microphone Meta-Arrays for Consumer Electronics. *IEEE Trans. Consum. Electron.* **2023**, *69*, 640–648. [CrossRef]
58. Rocchi, N.; Toscani, A.; Pinardi, D.; Binelli, M.; Chiesi, L.; Farina, A.; Bonomi, E.; Tronchin, L. A Modular, Low Latency, A^2B-based Architecture for Distributed Multichannel Full-Digital Audio Systems. In Proceedings of the 2021 Immersive and 3D Audio: From Architecture to Automot (I3DA), Bologna, Italy, 8–10 September 2021; IEEE: New York, NY, USA, 2021; pp. 1–8. [CrossRef]
59. Rocchi, N.; Toscani, A.; Chiorboli, G.; Pinardi, D.; Binelli, M.; Farina, A. Transducer Arrays over A^2B Networks in Industrial and Automotive Applications: Clock Propagation Measurements. *IEEE Access* **2021**, *9*, 118232–118241. [CrossRef]
60. Bertet, S.; Daniel, J.; Moreau, S. 3D Sound Field Recording with Higher Order Ambisonics—Objective Measurements and Validation of Spherical Microphone. In Proceedings of the Audio Engineering Society Convention 120, Paris, France, 20–23 May 2006. Available online: http://www.aes.org/e-lib/browse.cfm?elib=13661 (accessed on 12 March 2025).
61. Fredianelli, L.; Pedrini, G.; Bolognese, M.; Bernardini, M.; Fidecaro, F.; Licitra, G. Features for Evaluating Source Localization Effectiveness in Sound Maps from Acoustic Cameras. *Sensors* **2024**, *24*, 4696. [CrossRef]
62. Csóka, B.; Fiala, P.; Rucz, P. Tracking Sound Sources with Microphone Arrays and Beamforming Algorithms. In Proceedings of the Proceedings of the 10th Convention of the European Acoustics Association Forum Acusticum 2023, Torino, Italy, 11–15 September 2023; European Acoustics Association: Turin, Italy, 2024; pp. 1115–1122. [CrossRef]